

Intrinsic spin-orbit torque mechanism for deterministic all-electric switching of noncollinear antiferromagnets

Yiyuan Chen^{†,1,2,3,4} Z. Z. Du^{†,1,3,4} Hai-Zhou Lu,^{1,2,3,4,*} and X. C. Xie^{5,6,7}

¹Shenzhen Institute for Quantum Science and Engineering and Department of Physics, Southern University of Science and Technology (SUSTech), Shenzhen 518055, China

²Quantum Science Center of Guangdong-Hong Kong-Macao Greater Bay Area (Guangdong), Shenzhen 518045, China

³Shenzhen Key Laboratory of Quantum Science and Engineering, Shenzhen 518055, China

⁴International Quantum Academy, Shenzhen 518048, China

⁵International Center for Quantum Materials, School of Physics, Peking University, Beijing100871, China

⁶Institute for Nanoelectronic Devices and Quantum Computing, Fudan University, Shanghai 200433, China

⁷Hefei National Laboratory, Hefei 230088, China

Using a pure electric current to control kagome noncollinear antiferromagnets is promising in information storage and processing, but a full description is still lacking, in particular, on intrinsic (i.e., no external magnetic fields or external spin currents) spin-orbit torques. In this work, we self-consistently describe the relations among the electronic structure, magnetic structure, spin accumulations, and intrinsic spin-orbit torques, in the magnetic dynamics of a noncollinear antiferromagnet driven by a pure electric current. Our calculation can yield a critical current density comparable with those in the experiments, when considering the boost from the out-of-plane magnetic dynamics induced by the current-driven spin accumulation on individual magnetic moments. We stress the parity symmetry breaking in deterministic switching among magnetic structures. This work will be helpful for future applications of noncollinear antiferromagnets.

Introduction. - antiferromagnets have been expected to replace the ferromagnets in information storage and processing, because they are robust against perturbations guaranteed by their zero stray field and have higher energy scale for ultrafast performance. However, it is hard to read out ordinary PT -symmetric antiferromagnets (e.g., $\uparrow\downarrow\uparrow\downarrow$...) because of their weak magnetization. Recently, kagome noncollinear antiferromagnets [Fig. 1(a)] have attracted increasing attention, because they have strong anomalous Hall, Nernst, and magneto-optical Kerr effects [1–11] to serve as readout signals.

Using only pure electric current to manipulate the kagome antiferromagnets can greatly facilitate device applications [12]. Nevertheless, so far the theories mainly focus on their anomalous [4, 8, 13–16] and spin [17, 18] Hall effects, and their magnetic dynamics driven by the extrinsic mechanisms, i.e., through an extrinsic spin current assisted by a magnetic field [19–21]. A theory that fully describes the magnetic dynamics driven by a pure electric current is still lacking, in particular, on their intrinsic spin-orbit torques.

In this Letter, we theoretically show how a kagome noncollinear antiferromagnet can be manipulated by the intrinsic spin-orbit torques from the spin accumulations induced by a pure electric current, following the microscopic mechanism below [Fig. 1(b-d)].

Pure electric current	\Rightarrow	Spin accumulation	\Rightarrow	Intrinsic spin-orbit torque	\Rightarrow	Magnetic dynamics of moments
-----------------------	---------------	-------------------	---------------	-----------------------------	---------------	------------------------------

We self-consistently calculate the electronic structure, magnetic structure, spin accumulations, and intrinsic spin-orbit torques (Fig. 2). We point out the significance

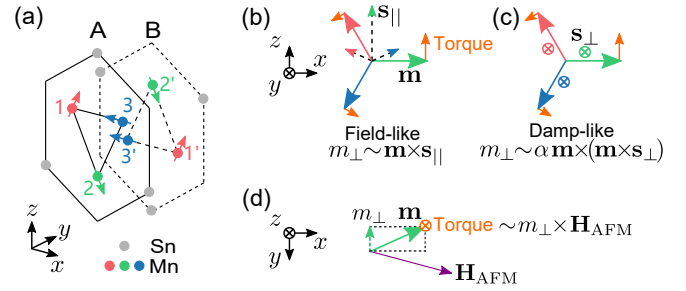


FIG. 1. (a) A kagome noncollinear antiferromagnet, e.g., Mn_3Sn . The red, green, and blue arrows stand for the three Mn moments \mathbf{m} (1-3 on layer A, 1'-3' on layer B) in the unit cell of a single kagome layer. [(b) and (c)] The spin-orbit coupling converts a pure electric current into spin accumulations (dashed arrows for in-plane \mathbf{s}_{\parallel} and \otimes for out-of-plane \mathbf{s}_{\perp}). The spin accumulations induce an out-of-plane component m_{\perp} of \mathbf{m} , via the field-like torque $\mathbf{m} \times \mathbf{s}_{\parallel}$ for \mathbf{s}_{\parallel} in (b) or via the damp-like torque $\alpha \mathbf{m} \times (\mathbf{m} \times \mathbf{s}_{\perp})$ for \mathbf{s}_{\perp} in (c). (d) For a moment \mathbf{m} , its antiferromagnetic interaction with other two moments acts like an effective field \mathbf{H}_{AFM} and $m_{\perp} \times \mathbf{H}_{AFM}$ gives the torques (orange arrows and \otimes) that rotate the magnetic structure in the kagome (x - z) plane. The field-like torque in (b) is dominant, because of the small damping constant α in front of the damp-like torque in (c).

of parity symmetry breaking in deterministic switching (Fig. 3). Our calculation can yield a critical current density comparable with those in the experiments (Fig. 4), when considering the boost from the out-of-plane magnetic dynamics induced by the current-driven spin accumulation on individual magnetic moments. Our description of the magnetic dynamics of the kagome noncollinear antiferromagnet will be helpful for future applications.

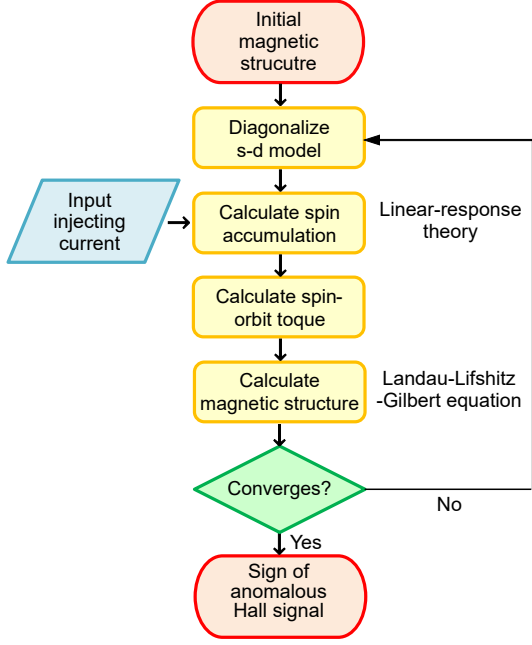


FIG. 2. The flowchart of the numerical simulation. We start by assuming an initial magnetic structure described by Eq. (1), which serves as local magnetic fields in the s - d model Eq. (7). Then, we use Eqs. (4) and (5) to calculate the spin accumulations on the Mn atoms at a given injecting current Eq. (6) and use Eq. (3) to calculate the magnetic torques of the spin accumulations in the Landau-Lifshitz-Gilbert equation Eq. (2), which generates a new magnetic structure. The steps are iterated until the magnetic structure converges, then the sign of the Hall signal can be determined by φ_2 .

Intrinsic spin-orbit torques. - First, we illustrate the spin-orbit torques from the spin accumulations induced by the pure electric current. The noncollinear antiferromagnet Mn_3Sn is formed by stacked bilayers along the c (y here) axis (Fig. 1). One layer in the bilayer is the inversion of the other, composed of a Mn kagome lattice and a Sn hexagonal lattice. In the unit cell of the Mn lattice, the magnetic moments of the three Mn atoms are rotated with respect to each other by nearly 120° , forming a noncollinear antiferromagnetic structure (Sec. S1 of [22]). The unit moment \mathbf{m}_a on Mn atom a is governed by [15]

$$H_m = 2 \sum_{ab} [J_m \mathbf{m}_a \cdot \mathbf{m}_b + D \hat{\mathbf{y}} \cdot (\mathbf{m}_a \times \mathbf{m}_b)] - K \sum_a (\hat{\mathbf{e}}_a \cdot \mathbf{m}_a)^2, \quad (1)$$

where $a, b \in \{1, 2, 3\}$ index the three Mn atoms in the unit cell, the first summation runs over the combinations $ab \in \{12, 23, 31\}$. The nearest neighbor Heisenberg interaction J_m and Dzyaloshinskii-Moriya interaction D describe a perfect triangular noncollinear antiferromagnetic structure with exactly 120° between the Mn magnetic

moments. The anisotropy K term breaks the in-plane $U(1)$ symmetry and leads to six stable positions to which the magnetic structure tends to relax [15] (see Fig. 4), $\hat{\mathbf{e}}_a$ represents the anisotropic axis for \mathbf{m}_a . The injected current has to exert enough spin-orbit torques to overcome the six stable positions for switching.

The dynamics of the magnetic moments \mathbf{m}_a is described by the Landau-Lifshitz-Gilbert equation (Sec. S2A of Ref. [22])

$$(1 + \alpha^2) \dot{\mathbf{m}}_a = \frac{|\gamma|}{M_S} \mathbf{m}_a \times \frac{\delta H_m}{\delta \mathbf{m}_a} + \mathbf{T}_a + \alpha \mathbf{m}_a \times \left(\frac{|\gamma|}{M_S} \mathbf{m}_a \times \frac{\delta H_m}{\delta \mathbf{m}_a} + \mathbf{T}_a \right), \quad (2)$$

where $\gamma (< 0)$ is the gyromagnetic ratio of the electron, α denotes the Gilbert damping coefficient, the saturation moment of a Mn atom $M_S = 3\mu_B$ with μ_B the Bohr magneton, and \mathbf{T}_a is the spin-orbit torques induced by the electric current. Different from the extrinsic damp-like spin-orbit torques [23, 24] $\mathbf{T}_a \sim \mathbf{m}_a \times (\mathbf{m}_a \times \mathbf{s})$ caused by externally injected spin currents with a uniform spin \mathbf{s} , we can show that the exchange interactions between the Mn moments and current-induced spin accumulations (Sec. S2B of Ref. [22]) naturally give the intrinsic field-like spin-orbit torques [25, 26]

$$\mathbf{T}_a = \frac{2|\gamma|J_{sd}V_U}{M_S\hbar} \mathbf{m}_a \times \tilde{\mathbf{s}}_a, \quad (3)$$

where the torques from the divergence of spin current and spin-orbit coupling [26] have been taken into account, J_{sd} is the exchange interaction between the Mn moments and itinerant electron spins, V_U is the volume of the unit cell, and inter-layer antiferromagnetic interactions (e.g., 1-2' and 1-3') tend to synchronize the diagonal moments (i.e., 1 and 1') on two layers, so we use the averaged local spin accumulation density $\tilde{\mathbf{s}}_a = (\mathbf{s}_a + \mathbf{s}_{a'})/2$. With the help of the linear-response theory [27] (derivations in Sec. S3 of Ref. [22]), the local spin accumulation density on Mn atom a induced by a pure electric current are found to have two parts (d for diagonal and od for off-diagonal matrix elements of the operators v and σ)

$$\mathbf{s}_a^d = \frac{e\hbar}{2V} \tau \sum_{\nu, \mathbf{k}} \frac{\partial f_\nu}{\partial \epsilon_\nu} (\mathbf{E} \cdot \mathbf{v}_{\nu\nu}) \boldsymbol{\sigma}_{\nu\nu}^a, \quad (4)$$

$$\mathbf{s}_a^{od} = \frac{e\hbar^2}{2V} \sum_{\mu \neq \nu, \mathbf{k}} (f_\mu - f_\nu) \text{Im} \left[\frac{(\mathbf{E} \cdot \mathbf{v}_{\mu\nu}) \boldsymbol{\sigma}_{\nu\mu}^a}{(\epsilon_\mu - \epsilon_\nu)^2} \right], \quad (5)$$

where the current density \mathbf{j} injected along an arbitrary direction enters as an electric field

$$\mathbf{E} = \frac{m^*}{e^2 n_{3D} \tau} \mathbf{j}, \quad (6)$$

$e = -1.6 \times 10^{-19}$ Coulomb, m^* is the effective mass, n_{3D} is the carrier density, τ is the relaxation time. Under the driving electric current, the system will enter a

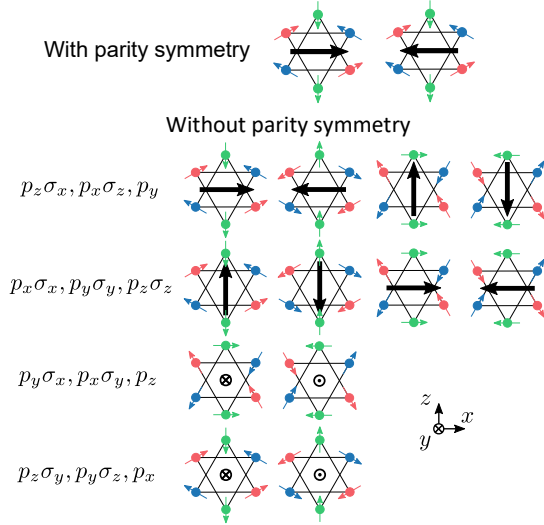


FIG. 3. Parity symmetry has to be broken for an electric current to deterministically manipulate the Mn moments, because the same magnetic structure is allowed for opposite electric currents (black arrow) under parity symmetry. We list all possible linear-momentum Hamiltonian terms that break parity symmetry and their resulting magnetic structures under the switching current.

nonequilibrium static state, in a time scale described by τ (usually 1-100 picoseconds) in the current-spin correlation Eq. (4). τ is much shorter than the nanosecond timescale of switching in Fig. 4, where the spin density is relaxed by the torque \mathbf{T}_a in Eq. (3) to transfer angular momenta to the magnetic structure. V is the volume of the system, f is the Fermi-Dirac distribution function, $\boldsymbol{\sigma}^a = (\sigma_x^a, \sigma_y^a, \sigma_z^a)$ are the Pauli matrices for the local spin density on Mn atom a , ϵ and v are the energy and group velocity operators, ν and μ label the energy bands, described by an s - d model (Sec. S4 of Ref. [22])

$$H_{sd} = J_{sd} \sum_{i,a,n,n'} \mathbf{m}_a \cdot \boldsymbol{\sigma}_{nn'} c_{ian}^\dagger c_{ian'} + H_e, \quad (7)$$

where J_{sd} is the exchange interaction between the Mn moments ($a \in \{1, 2, 3, 1', 2', 3'\}$) and spins of itinerant electrons ($n \in \{\uparrow, \downarrow\}$), and i indexes the unit cell. The itinerant electron part H_e needs to include parity symmetry breaking, as illustrated below.

Requirement of parity symmetry breaking. - The parity operation transforms the current (a radial vector) to the opposite direction while leaving the Mn moments (axial vectors) invariant, which means that an opposite current could also lead to the same final state of the Mn moments, so there is no one-to-one deterministic relation between the current direction and magnetizations of the Mn moments under parity symmetry (Fig. 3). This can also be seen from a symmetry analysis of Eqs. (4) and (5) (Sec. S5 of Ref. [22]). Required by parity symmetry breaking, we figure out all possible linear-momentum

TABLE I. Diagonal [Eq. (4)] and off-diagonal [Eq. (5)] spin accumulations on the diagonal lattice sites $(a, a') \in \{(1, 1'), (2, 2'), (3, 3')\}$, constrained by the symmetries of the model in Eq. (8) with two different parity symmetry breaking terms Δ_p^I and Δ_p^{II} . Here, $\parallel \in \{x, z\}$ and $\perp = y$ mean in and out of the kagome planes, respectively. P and T are the inversion and time-reversal operations, respectively, C_{2y} is the two-fold rotation around the y axis, and $\boldsymbol{\tau}_y$ is the translation along the y axis for half lattice constant $c/2$.

	Symmetry	Diagonal	Off-diagonal
$\Delta_p^I \neq 0$,	$T\{C_{2y} \boldsymbol{\tau}_y\}$	$(\mathbf{s}_d^a + \mathbf{s}_d^{a'})_{\parallel} \neq 0$	$(\mathbf{s}_{od}^a + \mathbf{s}_{od}^{a'})_{\parallel} = 0$
$\Delta_p^{II} = 0$		$(\mathbf{s}_d^a + \mathbf{s}_d^{a'})_{\perp} = 0$	$(\mathbf{s}_{od}^a + \mathbf{s}_{od}^{a'})_{\perp} \neq 0$
$\Delta_p^I = 0$,	$T\{PC_{2y} \boldsymbol{\tau}_y\}$	$(\mathbf{s}_d^a + \mathbf{s}_d^{a'})_{\parallel} = 0$	$(\mathbf{s}_{od}^a + \mathbf{s}_{od}^{a'})_{\parallel} \neq 0$
$\Delta_p^{II} \neq 0$		$(\mathbf{s}_d^a + \mathbf{s}_d^{a'})_{\perp} \neq 0$	$(\mathbf{s}_{od}^a + \mathbf{s}_{od}^{a'})_{\perp} = 0$

Hamiltonian terms that break parity symmetry, as shown in Fig. 3. To construct the itinerant electron Hamiltonian H_e , we choose to add $p_y\sigma_y$ term with magnitude Δ_p^I or p_y term with magnitude Δ_p^{II} to break parity symmetry in the previously-proposed three-dimensional (3D) Weyl model [16]. Its tight-binding model reads

$$H_e^W = \sum_{\langle ia,jb \rangle_{\parallel}} c_{ia}^\dagger t_{ia,jb} c_{jb} + \sum_{\langle ia,jb \rangle_{\perp}} c_{ia}^\dagger t'_{ia,jb} c_{jb} + \sum_{\langle ia,jb \rangle} c_{ia}^\dagger \mathbf{i}(\Delta_p^I \sigma_y + \Delta_p^{II}) \text{sgn}(\hat{\mathbf{y}} \cdot \hat{\mathbf{d}}_{ia,jb}) c_{jb}, \quad (8)$$

where $c_{ia} = (c_{ia\uparrow}, c_{ia\downarrow})^T$, \parallel and \perp distinguish the intra-layer and inter-layer nearest neighbor sites, $t_{ia,jb} = t \exp[\pm i\alpha_1 \sigma_y / 2]$, with $+$ for $ab \in \{12, 23, 31, 1'2', 2'3', 3'1'\}$ and $-$ for $ab \in \{21, 31, 13, 2'1', 3'2', 1'3'\}$, $t'_{ia,jb} = t \exp[-\frac{i}{2} \text{sgn}(\hat{\mathbf{d}}_{ia,jb} \cdot \hat{\mathbf{y}}) \alpha_2 (\cos \theta \hat{\mathbf{d}}_{ia,jb}^{\parallel} + \sin \theta \hat{\mathbf{y}}) \cdot \boldsymbol{\sigma}]$. α_1 , α_2 , and θ are the model parameters. With the help of symmetry analysis, we find that for $\Delta_p^I \neq 0$, the non-zero diagonal term of spin accumulations are in-plane and non-zero off-diagonal term of spin accumulations are out of plane; for $\Delta_p^{II} \neq 0$, the non-zero diagonal term of spin accumulations are out of plane and non-zero off-diagonal term of spin accumulations are in plane. Another choice to break parity symmetry is a 2D Rashba model with $p_x\sigma_z - p_z\sigma_x$ term, as compared in Sec. S5 of Ref. [22].

Complete simulation of magnetic dynamics. - Following the steps in Fig. 2), we perform numerical simulations to show how the pure electric current switches the magnetic structure of the kagome non-collinear antiferromagnet. The results for one of the Weyl model ($\Delta_p^I \neq 0$, $\Delta_p^{II} = 0$) are shown in Fig. 4 (a), measured by the magnetic moment angle of one of the Mn atoms φ_2 . As the current along the $+z$ ($-z$) direction is turned on and above a critical current density, the magnetic structure can be fully polarized to a metastable position at $\varphi_2 = \pi/2$ ($\varphi_2 = -\pi/2$). As the current is turned off, the magnetic structure relaxes to the nearest one of the six stable positions. More simulations for the other Weyl

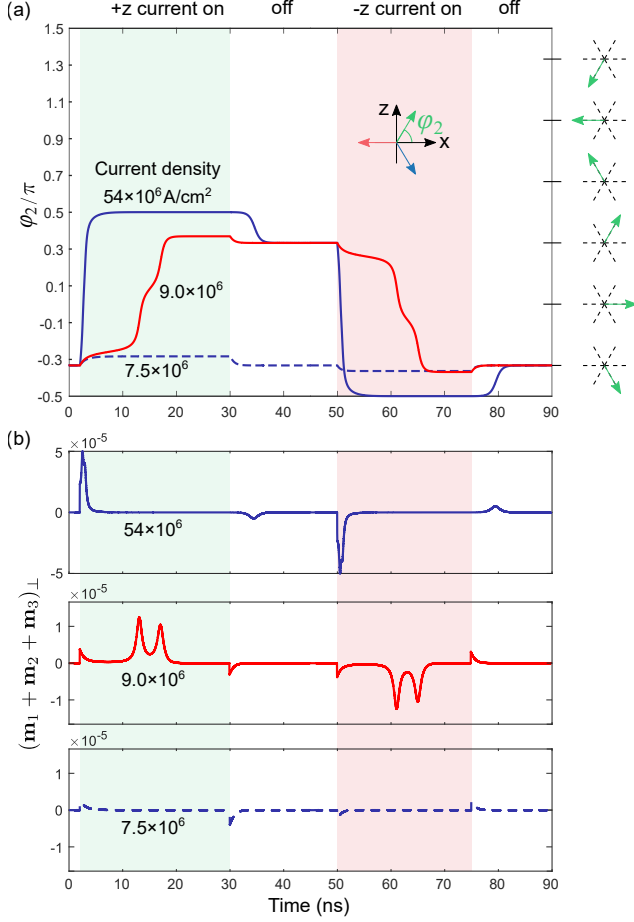


FIG. 4. (a) Simulated magnetic dynamics of Mn_3Sn in terms of the moment angle φ_2 (inset) of the Mn atom 2, driven by a pure electric current below (7.5×10^6), well above (54×10^6), and at the critical current density ($j \sim 9.0 \times 10^6$ A/cm², comparable with those in the experiment [12]), for the Weyl model ($\Delta_p^I = 0.075$ eV, $\Delta_p^{II} = 0$) in Eq. (8); From 2 through 30 ns (from 50 through 75 ns), j is along the $+z$ ($-z$) direction. In absence of j , φ_2 tends to relax at one of the six stable positions marked on the right axis. (b) The total out-of-plane magnetic moment of all three Mn atoms $(\mathbf{m}_1 + \mathbf{m}_2 + \mathbf{m}_3)_\perp$ for the three current densities in (a). The parameters are $t=0.25$ eV, $J_{sd}=0.125$ eV, $\alpha_1 = \alpha_2 = \pi/5$, $\theta = \pi/4$ [16], $\tau = \hbar/2\Gamma$ with $\Gamma=1.25$ meV, $m^* = 9.1 \times 10^{-31}$ kg, $n_{3D} = 6 \times 10^{23}/\text{cm}^3$, $J_m=23$ meV, $D=1.6$ meV, $K=0.17$ meV, $\alpha = 0.003$ [19].

model and Rashba model can be found in Fig. S8 of Sec. S4C in Ref. [22].

Our simulations yield a low critical current density comparable with those in the experiments [12], for two reasons. First, we reveal a boost from the out-of-plane magnetic dynamics, similar to a case in the collinear antiferromagnets [28]. According to our simulations, the torque is dominantly contributed by the scenario in Fig. 1(b), where, taking Mn 2 for example (\mathbf{m}), its current-induced in-plane spin accumulation \mathbf{s}_\parallel can induce an out-of-plane component m_\perp under the field-like torque

$\mathbf{m} \times \mathbf{s}_\parallel$, as shown by Fig. 1(b). For Mn 2, its antiferromagnetic interactions with other two Mn moments [i.e., $(|\gamma|/M_S)\mathbf{m}_a \times (\delta H_m/\delta \mathbf{m}_a)$ in Eq. (2)] act like an effective field \mathbf{H}_{AFM} and $m_\perp \times \mathbf{H}_{\text{AFM}}$ gives the torque in the kagome plane, as shown by the orange \otimes in Fig. 1(d) and orange arrow in Fig. 1(b). This out-of-plane dynamics is efficient, because $\mathbf{H}_{\text{AFM}} \sim 2J_m/M_s \sim 264$ Tesla, is pretty strong. This out-of-plane magnetic dynamics also occurs to Mn 1 and Mn 3. When the total out-of-plane moments of three Mn atoms $(\mathbf{m}_1 + \mathbf{m}_2 + \mathbf{m}_3)_\perp > 0$ (< 0), the entire magnetic structure rotates counter-clockwise (clockwise) among stable and metastable positions. Fig. 4(b) shows that a peak of $(\mathbf{m}_1 + \mathbf{m}_2 + \mathbf{m}_3)_\perp$ always emerges along with a transition in Fig. 4(a), indicating the significance of the boost from the out-of-plane magnetic dynamics. By contrast, although the damp-like torque $\mathbf{m} \times (\mathbf{m} \times \mathbf{s}_\perp)$ from out-of-plane spin accumulation \mathbf{s}_\perp in Fig. 1(c) can also induce the out-of-plane moment, it is much smaller because of the small damping constant α in front (see Sec. S2C in Ref. [22]). Second, we assume that the Mn atoms feel different fields locally produced by the spin accumulations in the simulation. In contrast, if we assume that the Mn atoms feel the same field collectively (like the torques from the extrinsically injected spin currents [19]), the critical current density has to be about three orders larger (see Fig. S13 in Sec. S7B of Ref. [22]). The sharp difference can be understood as follows. The above-mentioned $(\mathbf{m}_1 + \mathbf{m}_2 + \mathbf{m}_3)_\perp$ is proportional to $\mathbf{m}_1 \times \mathbf{s}_1 + \mathbf{m}_2 \times \mathbf{s}_2 + \mathbf{m}_3 \times \mathbf{s}_3$ under the different-field assumption, and $(\mathbf{m}_1 + \mathbf{m}_2 + \mathbf{m}_3) \times \mathbf{s}$ in the same-field assumption, where $\mathbf{s} = \mathbf{s}_1 + \mathbf{s}_2 + \mathbf{s}_3$, comparable with each of \mathbf{s}_a (see Fig. S9 of Ref. [22]). For the noncollinear 120° texture of Mn_3Sn , $\mathbf{m}_1, \mathbf{m}_2, \mathbf{m}_3$ nearly cancel with each other, and $\mathbf{m}_1 + \mathbf{m}_2 + \mathbf{m}_3$ is about $0.01\mu_B$ [19], three orders smaller than that of $\mathbf{m}_i \sim 3\mu_B$, so the critical current density under the same-field assumption is about three orders larger.

Our simulations also reveal many microscopic details. For the current density of 54×10^6 in Fig. 4(a), after turning off the current, it takes a few ns to transit to another state. This feature appears when the magnetic structure is very close to a metastable position (e.g., $\varphi_2 = \pi/2$) at the middle of two neighbor stable positions ($\varphi_2 = \pi/3$ and $2\pi/3$). The argument is, at exactly the metastable position, there is no preference of falling to any one the two equivalent neighbor stable positions, so it takes a longer time to break the detailed balance to escape from the vicinity of the metastable position. To illustrate this, we present the simulations starting from slightly below, extremely close to, and slightly above a metastable position (Fig. S15 in Ref. [22]).

[†]Y.C. and Z.Z.Du contributed to the work equally. We thank helpful discussions with Kaiyou Wang. This work was supported by the National Key R&D Program of China (2022YFA1403700), Innovation Program for Quantum Science and Technology (2021ZD0302400), the

National Natural Science Foundation of China (11925402 and 12004157), Guangdong province (2020KCXTD001 and 2016ZT06D348), and the Science, Technology and Innovation Commission of Shenzhen Municipality (ZDSYS20170303165926217, JAY20170412152620376, and KYTDPT20181011104202253). The numerical calculations were supported by Center for Computational Science and Engineering of SUSTech.

* Corresponding author: luhz@sustech.edu.cn

- [1] S. Nakatsuji, N. Kiyohara, and T. Higo, “Large anomalous Hall effect in a non-collinear antiferromagnet at room temperature”, *Nature* **527**, 212 (2015).
- [2] M. Ikhlas, T. Tomita, T. Koretsune, M.-T. Suzuki, D. Nishio-Hamane, R. Arita, Y. Otani, and S. Nakatsuji, “Large anomalous Nernst effect at room temperature in a chiral antiferromagnet”, *Nature Physics* **13**, 1085 (2017).
- [3] X. Li, L. Xu, L. Ding, J. Wang, M. Shen, X. Lu, Z. Zhu, and K. Behnia, “Anomalous Nernst and righi-leduc effects in Mn_3Sn : Berry curvature and entropy flow”, *Phys. Rev. Lett.* **119**, 056601 (2017).
- [4] H. Chen, Q. Niu, and A. H. MacDonald, “Anomalous Hall effect arising from noncollinear antiferromagnetism”, *Phys. Rev. Lett.* **112**, 017205 (2014).
- [5] N. Kiyohara, T. Tomita, and S. Nakatsuji, “Giant anomalous Hall effect in the chiral antiferromagnet Mn_3Ge ”, *Phys. Rev. Applied* **5**, 064009 (2016).
- [6] A. K. Nayak, J. E. Fischer, Y. Sun, B. Yan, J. Karel, A. C. Komarek, *et al.*, “Large anomalous Hall effect driven by a nonvanishing Berry curvature in the non-collinear antiferromagnet Mn_3Ge ”, *Science Advances* **2** (2016), [10.1126/sciadv.1501870](https://doi.org/10.1126/sciadv.1501870).
- [7] Z. H. Liu, Y. J. Zhang, G. D. Liu, B. Ding, E. K. Liu, H. M. Jafri, *et al.*, “Transition from anomalous Hall effect to topological Hall effect in hexagonal non-collinear magnet Mn_3Ga ”, *Scientific Reports* **7** (2017), [10.1038/s41598-017-00621-x](https://doi.org/10.1038/s41598-017-00621-x).
- [8] Z. Q. Liu, H. Chen, J. M. Wang, J. H. Liu, K. Wang, Z. X. Feng, *et al.*, “Electrical switching of the topological anomalous Hall effect in a non-collinear antiferromagnet above room temperature”, *Nature Electronics* **1**, 172 (2018).
- [9] T. Ikeda, M. Tsunoda, M. Oogane, S. Oh, T. Morita, and Y. Ando, “Anomalous Hall effect in polycrystalline Mn_3Sn thin films”, *Applied Physics Letters* **113**, 222405 (2018).
- [10] T. Higo, D. Qu, Y. Li, C. L. Chien, Y. Otani, and S. Nakatsuji, “Anomalous Hall effect in thin films of the Weyl antiferromagnet Mn_3Sn ”, *Applied Physics Letters* **113**, 202402 (2018).
- [11] T. Higo, H. Man, D. B. Gopman, L. Wu, T. Koretsune, O. M. J. V. T. Erve, *et al.*, “Large magneto-optical Kerr effect and imaging of magnetic octupole domains in an antiferromagnetic metal”, *Nature Photonics* **12**, 73 (2018).
- [12] Y. Deng, X. Liu, Y. Chen, Z. Du, N. Jiang, C. Shen, E. Zhang, H. Zheng, H.-Z. Lu, and K. Wang, “All-electrical switching of a topological non-collinear antiferromagnet at room temperature”, *National Science Review* (2023), [10.1093/nsr/nwac154](https://doi.org/10.1093/nsr/nwac154).
- [13] R. Shindou and N. Nagaosa, “Orbital ferromagnetism and anomalous Hall effect in antiferromagnets on the distorted fcc lattice”, *Phys. Rev. Lett.* **87**, 116801 (2001).
- [14] Y. Zhang, Y. Sun, H. Yang, J. Železný, S. P. P. Parkin, C. Felser, and B. Yan, “Strong anisotropic anomalous Hall effect and spin Hall effect in the chiral antiferromagnetic compounds Mn_3X ($X=Ge, Sn, Ga, Ir, Rh, \text{ and } Pt$)”, *Phys. Rev. B* **95**, 075128 (2017).
- [15] J. Liu and L. Balents, “Anomalous Hall effect and topological defects in antiferromagnetic Weyl semimetals: mn_3Sn/Ge ”, *Phys. Rev. Lett.* **119**, 087202 (2017).
- [16] S.-S. Zhang, H. Ishizuka, H. Zhang, G. B. Halász, and C. D. Batista, “Real-space Berry curvature of itinerant electron systems with spin-orbit interaction”, *Phys. Rev. B* **101**, 024420 (2020).
- [17] J. Železný, Y. Zhang, C. Felser, and B. Yan, “Spin-polarized current in noncollinear antiferromagnets”, *Phys. Rev. Lett.* **119**, 187204 (2017).
- [18] M. Kimata, H. Chen, K. Kondou, S. Sugimoto, P. K. Muduli, M. Ikhlas, *et al.*, “Magnetic and magnetic inverse spin Hall effects in a non-collinear antiferromagnet”, *Nature* **565**, 627 (2019).
- [19] H. Tsai, T. Higo, K. Kondou, T. Nomoto, A. Sakai, A. Kobayashi, *et al.*, “Electrical manipulation of a topological antiferromagnetic state”, *Nature* **580**, 608 (2020).
- [20] B. Pal, B. K. Hazra, B. Göbel, J.-C. Jeon, A. K. Pandeya, A. Chakraborty, *et al.*, “Setting of the magnetic structure of chiral kagome antiferromagnets by a seeded spin-orbit torque”, *Science Advances* **8**, eabo5930 (2022).
- [21] H. Xie, X. Chen, Q. Zhang, Z. Mu, X. Zhang, B. Yan, and Y. Wu, “Magnetization switching in polycrystalline Mn_3Sn thin film induced by self-generated spin-polarized current”, *Nature Communications* **13**, 5744 (2022).
- [22] See Supplemental Material for (Sec. S1) Magnetic structure, (Sec. S2) Landau-Lifshitz-Gilbert equation, (Sec. S3) Linear-response theory of current-spin correlations, (Sec. S4) Electronic Hamiltonian, (Sec. S5) Spin accumulations, (Sec. S6) Symmetry analysis of magnetic dynamics, and (Sec. S7) Supplemental discussions, which includes Refs. [12,15,16,18,19,27].
- [23] L. Liu, T. Moriyama, D. C. Ralph, and R. A. Buhrman, “Spin-torque ferromagnetic resonance induced by the spin Hall effect”, *Phys. Rev. Lett.* **106**, 036601 (2011).
- [24] J. Slonczewski, “Current-driven excitation of magnetic multilayers”, *Journal of Magnetism and Magnetic Materials* **159**, L1 (1996).
- [25] P. Haney, R. Duine, A. Núñez, and A. MacDonald, “Current-induced torques in magnetic metals: Beyond spin-transfer”, *Journal of Magnetism and Magnetic Materials* **320**, 1300 (2008).
- [26] Manchon, A., and S. Zhang, 2011, “Spin Torque in Magnetic Systems: Theory,” in Handbook of Spin Transport and Magnetism, edited by Evgeny Y. Tsymbal, and Igor Zutic (CRC Press, Boca Raton), Chap. 8, pp. 157–178..
- [27] G. D. Mahan, *Many-Particle Physics*, 3rd ed., Physics of Solids and Liquids (Springer Science & Business Media New York, 2000).
- [28] O. Gomonay, V. Baltz, A. Brataas, and Y. Tserkovnyak, “Antiferromagnetic spin textures and dynamics”, *Nature Physics* **14**, 213 (2018).